

Dynamic Grasping of Unknown Objects with a Multi-Fingered Hand

Yannick Burkhardt^{1,2,†}, Qian Feng^{1,2,†}, Karan Sharma¹, Zhaopeng Chen¹, Alois Knoll²

Abstract—An important prerequisite for autonomous robots is their ability to reliably grasp a wide variety of objects. Most state-of-the-art systems employ specialized or simple end-effectors, such as two-jaw grippers, which severely limit the range of objects to manipulate. Additionally, they conventionally require a structured and fully predictable environment while the vast majority of our world is complex, unstructured, and dynamic. This paper presents an implementation to overcome both issues. Firstly, the integration of a five-finger hand enhances the variety of possible grasps and manipulable objects. This kinematically complex end-effector is controlled by a deep learning based generative grasping network. The required virtual model of the unknown target object is iteratively completed by processing visual sensor data. Secondly, this visual feedback is employed to realize closed-loop servo control which compensates for external disturbances. Our experiments on real hardware confirm the system’s capability to reliably grasp unknown dynamic target objects without a priori knowledge of their trajectories. To the best of our knowledge, this is the first method to achieve dynamic multi-fingered grasping for unknown objects. A video of the experiments is available at <https://youtu.be/Ut28yM1gnvI>.

I. INTRODUCTION

Grasping unknown, moving objects presents numerous challenges: the computationally intensive methods used to deduce grasping strategies solely on sensor data from the environment must be repetitively executed in real-time to allow continuous adaption to the changing object pose. Additionally, there are many sources of error resulting in grasp failure, including tracking loss, inaccurate target segmentation as well as a collision between the robot and the dynamic environment. For these reasons, most previous works simplify this complex problem with prior assumptions regarding the target, its trajectory, or the grasp.

All existing approaches on dynamic grasping we found use two- or three-jaw grippers which are controlled by a single degree of freedom (DoF) to open or close. The system presented in this paper employs a multi-fingered hand: the 15 DoF anthropomorphic DLR-HIT Hand II [1]. While this high-dimensional end-effector is more complex to control, it allows manipulation of an increased variety of objects as demonstrated in various works [2], [3]. For this hand, the grasp sampling and evaluation framework *Five-finger Hand Net (FFHNet)* [4] was developed. Since it is the first real-time capable deep learning based system for multi-fingered grasping, we demonstrate the potential of employing it in a closed control loop for grasping unknown objects. Figure 1 shows successful grasps from our conducted experiments.

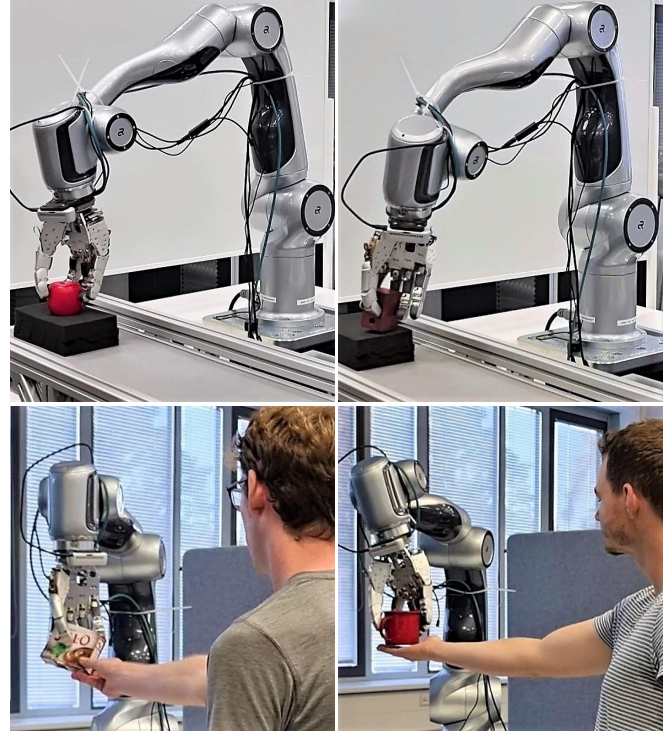


Fig. 1: Successful grasps in the conveyor belt experiment with target velocities of 220 mm/s for the apple (top left) and 180 mm/s for the foam brick (top right). Human-to-robot handovers of the pudding box (bottom left) and the mug (bottom right).

This novel approach fulfills the following five properties to achieve robust dynamic grasp execution: (1) By processing camera feedback, the closed-loop servo controller increases the robustness regarding sensor noise, model error, and physical disturbances. This enables the system to track and grasp moving objects. (2) Every part of the system is real-time capable (≥ 30 Hz). (3) During the grasp approach phase, sensor observations are combined to improve the virtual target model required for grasp generation. This provides the basis to fully exploit the capabilities of multi-fingered grasping since it facilitates the inference of reliable grasps compared to an evaluation of the most recent observation only. Additionally, since our system relies on a single-camera view, this allows an estimation of a suitable grasp pose in the absence of useful sensor feedback, e.g., due to occlusions. (4) To achieve high flexibility, the system is designed such that it requires little prior knowledge and is not coupled to predefined classes of a data set: both tracking and grasp generation perform well on unseen objects. (5) Lastly, employing a multi-fingered hand enables better manipulability and higher flexibility compared to standard two-jaw grippers. This work’s contributions can be summarized as follows:

¹Agile Robots AG, qian.feng@agile-robots.com

²Chair for Robotics, Artificial Intelligence and Embedded Systems, Technical University of Munich

[†]These authors contributed equally to this work.

- Our novel method is, to the best of our knowledge, the first to enable multi-fingered grasping of dynamic targets. It jointly integrates state-of-the-art image processing, grasp planning, and robot control methods.
- We present an approach to filter and combine the visual tracking results to create a virtual target model online without prior knowledge of the target’s movement.
- Our novel metric for dynamic grasping updates the target grasp from a set that is continuously re-generated in real-time. It facilitates the simultaneous evaluation of multiple factors influencing grasp success and offers an interface for potential future extensions.
- We demonstrate our system’s capabilities to grasp various moving objects in different real-world experiments.

II. RELATED WORK

In contrast to the system presented in this paper, all publications in this section use grippers which are controlled by a single DoF. This also applies to the works employing three-jaw grippers since they couple all fingers to open or close [5]–[8]. Additionally, they impose restrictions on the target object to be graspable with this finger configuration. Instead, we employ a 15-DoF multi-fingered hand with superior manipulation capabilities and enable grasping of truly unknown objects.

Early works are limited to the execution of pre-programmed grasps for a single known object. While initially the target’s trajectory must be known a priori [9], [10], this simplification is later omitted [11]–[13]. Also, more recent approaches constrain the target and its pose to ensure the stability of a pre-programmed grasp [5], [6], [14]. Some additionally require the target to be known or to fulfill specific geometric properties [6], [14]. Another approach greatly simplifies visual tracking and grasp planning by marking the grasp pose with an Apriltag on the target [15].

Modern methods often use data-driven models to generate grasps. Some systems rely only on the most recent observation of a depth camera and discard all structural information from previous time steps [16]–[18]. Without a virtual model of the unknown target, they depend on always reliable camera data. This cannot be guaranteed in case of occlusions, unclear perspectives of the target, or inaccurate sensor feedback when the camera’s minimum depth range is undershot. While these implementations can handle changes in the target pose as it is approached, they require a static target directly before and during the execution of the grasp.

In another approach, the object’s model is not created online but requires a preceding time-inefficient scanning phase [19]. To avoid the necessity of real-time capable grasp generation, some systems use pre-generated sets of grasps and continuously re-rank these grasps during object tracking based on the target object’s movement [19]–[21]. However, this implies a priori knowledge of the target’s geometrical properties which does not apply to the approach presented in this paper. Also, the pre-processing step to generate grasps significantly increases process times.

A recent work to enable dynamic grasping by predicting the target’s movement does not generalize to unknown objects nor arbitrary trajectories [22]. The system AnyGrasp cannot adjust the grasp online based on visual feedback, and its speed of 7 Hz violates the real-time constraint, restricting the target’s movements to be slow and predictive [23].

Some works address dynamic grasping in the context of human-to-robot handovers using visual feedback [24], [25]. Since these implementations assume the human’s cooperation during the handover, they can at most handle minor target movements because they either do not update the grasp at all or only at a slow rate of 5 Hz.

Other approaches apply Deep Reinforcement Learning to the dynamic grasping problem [7], [8], [26]. However, all of them greatly reduce the grasp generation complexity by only considering spherical or cubic objects. Additionally, they further simplify the problem by either employing Apriltags for object detection [7], report a significant gap in the grasp success rate between simulated and real experiments [26], or exclusively evaluate their model in simulation [8].

Our model overcomes the mentioned limitations of the existing approaches by employing closed-loop servo control and target model generation in real-time to achieve five-fingered grasping of unknown dynamic targets.

III. METHOD

The control system is divided into the two processes *Target Model Generation* and *Grasp Control* as indicated in Figure 2. They run asynchronously to avoid blocking and to enable efficient recovery after errors such as tracking loss.

A. Target Model Generation

To create a point cloud model representing the target object, the camera feedback is processed. The depth camera attached to the robot’s end-effector (eye-in-hand configuration) provides a color and depth data stream. After initialization with a bounding box, the target object is segmented from subsequent color images by a visual object tracker as long as it stays in the camera’s observable space. In this work, the transformer-based model *TransT.M* [26] is chosen. As the winner of the VOT-RT2021 [27] challenge, it offers state-of-the-art robustness and accuracy for a huge diversity of objects while obeying real-time constraints.

Upon alignment of the camera’s color and depth data, the segmentation mask provided by the tracker is applied to the depth image, resulting in the segmentation of the target object’s surface structure. This depiction is converted to a point cloud. To avoid confusion, this point cloud directly generated from the camera data is called *observation* point cloud \mathbf{P}_t at time step t . The point cloud created by post-processing and merging the observation point clouds is called *model* point cloud \mathbf{Q}_t . The model point cloud represents the object from all observed perspectives.

Due to sensor noise and imperfections in the segmentation mask, a small number of undesired points might be also included in the observation point cloud. To minimize the amount of these faulty data in the model point cloud,

the observation point cloud is post-processed before being merged with the model point cloud.

Outliers belonging to the background are filtered out by removing all points whose z -coordinates $p_{t,i,z}$ differ from the median depth of the observation point cloud P_t by more than a threshold c_z

$$\mathbf{P}'_t = \bigcup_{\mathbf{P}_t} p_{t,i} [|p_{t,i,z} - \text{med}(\mathbf{P}_t)_z| \leq c_z]. \quad (1)$$

c_z determines the maximum length of the target's virtual representation in the camera's z -axis.

The transformation to align the observation point clouds from different time steps without a priori knowledge of the target movement can only be inferred by employing their structural information. This is achieved by registration with the *Iterative Closest Point* (ICP) algorithm [28], [29] which allows fast and precise approximation of the transformation between two point clouds by iteratively maximizing their overlap.

However, applying a local optimization algorithm such as ICP to noisy input data is error-prone. Since the resulting transformation is required to transform the model point cloud into the current camera frame, a false estimation can lead to imprecise grasps. To distinguish successful from unsuccessful ICP alignment, two criteria must be fulfilled:

- (1) The alignment's fitness score is sufficiently high.
- (2) The norms of the resulting translation and rotation between the two centered point clouds remain smaller than an upper bound. This implies a maximal relative velocity between the robot and the target.

If any of these conditions is violated, the recent observation is discarded. Otherwise, the model point cloud, as well as the previous n_s observation point clouds $\mathbf{P}_{t-\tau}$, are transformed into the current camera frame to match the pose of the recent observation point cloud \mathbf{P}_t .

As an additional post-processing step, the result is smoothed by selecting only points with correspondences in the previous n_s observations. When discretizing the continuous surface of the target object with a point cloud, the locations of single points in consecutive time steps differ due to the discretization grid depending on the camera and object pose. Therefore, a corresponding point is defined as one that lies in an ϵ -ball around the source point. Only if at least one point $p'_{t-\tau,j}$ can be found in every previous n_s observation point clouds $\mathbf{P}'_{t-\tau}$ with an Euclidean distance to the source point lower than a small positive constant ϵ , this source point $p'_{t,i}$ is considered for further processing

$$\mathbf{P}''_t = \bigcup_{\mathbf{P}'_t} p'_{t,i} [\forall \tau : \exists p'_{t-\tau,j} \in \mathbf{P}'_{t-\tau} : \|p'_{t,i} - p'_{t-\tau,j}\| < \epsilon]. \quad (2)$$

Finally, the post-processed observation point cloud \mathbf{P}''_t is merged with the model point cloud \mathbf{Q}_{t-1} to obtain an improved model point cloud \mathbf{Q}_t

$$\mathbf{Q}_t = \mathbf{Q}_{t-1} \cup \mathbf{P}''_t. \quad (3)$$

Grasps are generated based on this composed point cloud model. To allow efficient processing of the model point cloud

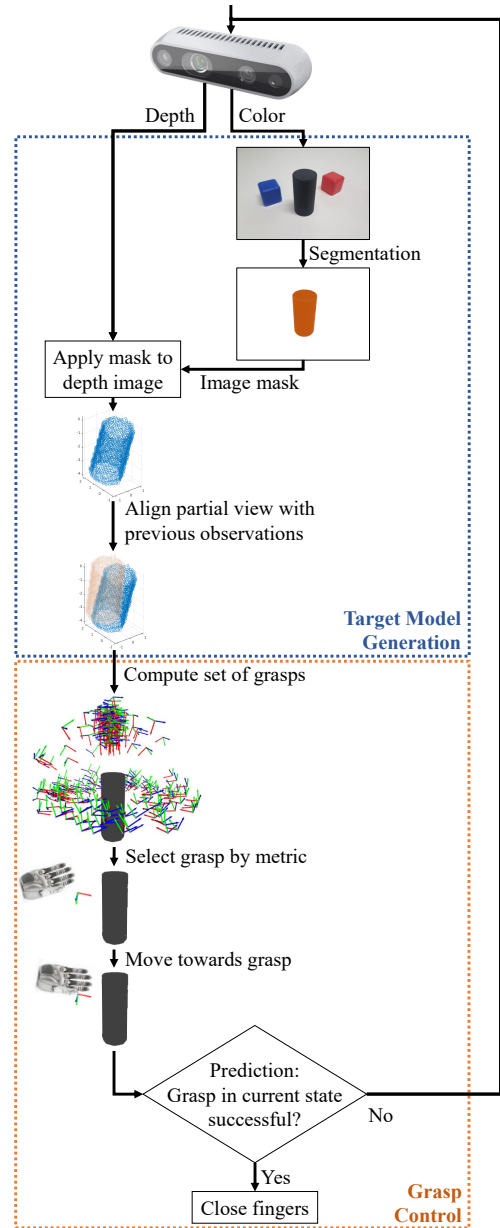


Fig. 2: Schematic representation of the control loop.

for machine learning algorithms, it is encoded with the Basis Point Set (BPS) [30]. The points are represented by their 1D distance to each fixed basis point instead of their 3D coordinates.

B. Grasp Control

The BPS-encoded point cloud constitutes the input for the generative grasping framework FFHNet [4]. It samples a set of grasps and assigns success predictions $s_{G,i}$. Every grasp is represented by its palm translation $\mathbf{t}_{G,i}$, its palm rotation matrix $\mathbf{R}_{G,i}$ and its finger configuration $\theta_{G,i}$.

The following sections describe the post-processing steps for selecting a suitable grasp and controlling the robot's movement to reach a pose where grasp execution is successful. Further steps are the estimation of the target's velocity and the estimation of the grasp pose in case of missing control feedback due to tracking or ICP failure.

1) *Grasp Metric*: From the generated grasps described by the set $\mathbb{G}_i = (\mathbf{t}_{G,i}, \mathbf{R}_{G,i}, \boldsymbol{\theta}_{G,i}, s_{G,i})$, one grasp is selected maximizing the metric

$$\mathbb{G}^* = \operatorname{argmax}_i \sum_j m_j(\mathbb{G}_i). \quad (4)$$

This metric combines the following quantities:

Predicted grasp success: To select a stable grasp, a high success prediction of FFHNet is required. This part is weighted with the constant c_0

$$m_0(\mathbb{G}_i) = c_0 s_{G,i}. \quad (5)$$

Pose difference: This part of the metric attempts to minimize the Euclidean distance between the robot's pose $(\mathbf{t}_R, \mathbf{r}_R)$ and the grasp pose $(\mathbf{t}_{G,i}, \mathbf{r}_{G,i})$ in axis-angle representation. The linear and angular offset are weighted with the constants $c_{1,l}$ and $c_{1,r}$

$$m_1(\mathbb{G}_i) = -c_{1,l} \|\mathbf{t}_{G,i} - \mathbf{t}_R\| - c_{1,r} \|\mathbf{r}_{G,i} - \mathbf{r}_R\|. \quad (6)$$

Shorter robot movements reduce the grasp execution time. This not only increases efficiency but also mitigates the failure risk caused by a target movement out of the robot's reachable space.

Kinematic feasibility: The robot must be able to kinematically reach the chosen grasp pose without any collisions. Grasps not fulfilling this property are neglected. Since checking the robot's inverse kinematics and collisions for all grasps at every time step is computationally inefficient, this constraint is enforced after evaluation of the grasp metric. If the chosen grasp is not reachable, the next best grasp is chosen and checked, until a valid grasp is found.

2) *Robot Control*: After evaluation of the grasp metric, the robot is moved towards the pose $(\mathbf{t}_G^*, \mathbf{R}_G^*)$ of the selected grasp \mathbb{G}^* . While minimizing the offset between the robot's current end-effector pose and the target end-effector pose, the object must remain in the camera's field of view to provide visual feedback for the control loop. Therefore, the control law for the end-effector's orientation is adjusted. As long as the translational error's norm of the end-effector position $\|\mathbf{t}_G^*\|$ is larger than a threshold c_O , the camera is aligned towards the target's center. Once this threshold is undershot, the desired orientation is linearly interpolated between the grasp orientation error \mathbf{r}_G^* and the alignment error between the camera center and object center \mathbf{r}_O . When $\|\mathbf{t}_G^*\|$ falls below another threshold c_G , exclusively the target grasp's orientation \mathbf{r}_G^* is approached

$$\tilde{\mathbf{r}}_G^* = \begin{cases} \mathbf{r}_O, & \|\mathbf{t}_G^*\| \geq c_O \\ \Delta g \cdot \mathbf{r}_O + (1 - \Delta g) \cdot \mathbf{r}_G^*, & \|\mathbf{t}_G^*\| \in (c_G, c_O) \\ \mathbf{r}_G^*, & \|\mathbf{t}_G^*\| \leq c_G \end{cases} \quad (7)$$

with $\Delta g = \frac{\|\mathbf{t}_G^*\| - c_G}{c_O - c_G}$, $c_O > c_G$.

All rotations are represented as axis-angle vectors.

With the resulting rotation $\tilde{\mathbf{r}}_G^*$, the desired Cartesian end-effector velocity $(\mathbf{v}_d, \boldsymbol{\omega}_d)^\top$ is calculated. The PD controller

$$\begin{pmatrix} \mathbf{v}_d \\ \boldsymbol{\omega}_d \end{pmatrix} = \begin{pmatrix} c_{p,v} \dot{\mathbf{t}}_G^* + c_{d,v} \mathbf{t}_G^* + \bar{\mathbf{v}}_G \\ c_{p,\omega} \tilde{\mathbf{r}}_G^* + c_{d,\omega} \dot{\tilde{\mathbf{r}}}_G^* \end{pmatrix} \quad (8)$$

with the empirically tuned control constants $c_{p,v}$, $c_{d,v}$, $c_{p,\omega}$, $c_{d,\omega}$ ensures fast grasp pose alignment. $\bar{\mathbf{v}}_G$ is the estimated velocity of the target.

3) *Grasp Execution*: The evaluator part of FFHNet models the relation between point cloud, grasp (pose and finger configuration), and success probability. Instead of a generated grasp, the current end-effector pose combined with the finger configuration of the recently selected grasp is fed to the neural network to predict the success probability of the current state. If an execution threshold is exceeded, the hand is closed to the predicted finger positions.

4) *Velocity Estimation*: The evolution of the target's position is tracked based on a fixed feature point on its surface. The object's velocity $\bar{\mathbf{v}}_G$ is estimated by processing the position of this feature point over time with a Kalman filter [31]. The estimated velocity is included in the control law in Equation 8. This allows the controller to behave similarly to a static grasping setup, assuming an accurate velocity estimate $\bar{\mathbf{v}}_G$. Additionally, this velocity is required to estimate a suitable grasp pose in the absence of useful control feedback.

5) *Grasp Pose Estimation*: The camera's field of view and depth range are limited and the ICP algorithm can provide incorrect transformations. Especially shortly before grasp execution, when the object is close to the camera, the risk of point cloud registration failure is increased. The camera's minimum depth range can lead to incorrect depth values, and its limited field of view can result in incorrect ICP registration because the object is only partially visible. E.g., a corner of a partially observed box can be aligned with any of the box corners since their structure is similar.

When these wrong transformations are filtered out, the control feedback is missing. Then, the target grasp is updated by moving it according to the estimated object velocity. A successful grasp in the absence of control feedback over multiple consecutive time steps requires a highly accurate velocity estimation.

IV. EXPERIMENTS

To demonstrate the method's capabilities, two experiments are carried out. At first, the target objects are grasped on a conveyor belt which moves at different linear velocities between 0 and 220 mm/s. The velocity of the conveyor belt as well as the direction of movement are unknown to the system and must be estimated online. The second experiment is a human-to-robot handover. This setup is challenging due to the nonlinear motions that humans perform. Figure 1 and the accompanying video show grasps from the experiments.

The target items are displayed in Figure 3. They are a subset of the *Yale-CMU-Berkeley (YCB)* object set [32] which was omitted during the training of FFHNet. Therefore, all of the target objects are unknown to the system.

The hardware used for the experiments is the 7 DoF robot manipulator *Agile Robots Diana 7*, the *DLR-HIT Hand II* [1], and the depth camera *Intel RealSense D435*. These components are controlled by a computer equipped with a *NVIDIA GeForce RTX 3070 Ti* graphics card.



Fig. 3: The ten YCB objects used in the experiments (left to right): sugar box, pudding box, gelatin box, mustard bottle, apple, mug, baseball, cup, foam brick, Rubik’s cube.

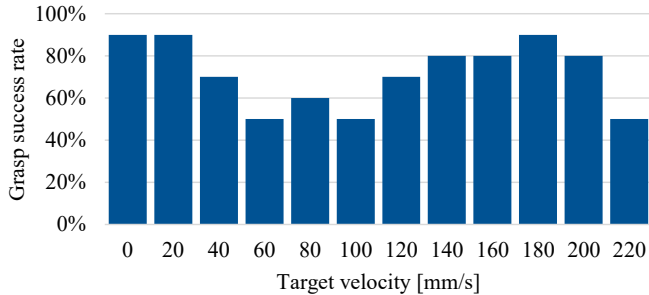


Fig. 4: Results of the conveyor belt experiment.

A. Grasping Objects on a Conveyor Belt

In this experiment, the ten target objects are grasped while moving linearly on a conveyor belt. Every object is grasped once for every speed increment of 20 mm/s between 0 and 220 mm/s. Figure 4 shows the grasping success rates for the respective conveyor belt velocities. For 120 grasp attempts, an average success of 71.7% is achieved. The diagram indicates that the system works reliably with success rates of 80–90% for target velocities slower than 20 mm/s and between 140 and 200 mm/s. Impressively, there is no performance degradation at these high speeds compared to static grasping, which shows the power of our implementation. However, the success rates drop to 50–60% for target speeds between 60 and 100 mm/s. We confirmed that tracking, target model generation, robot control, and velocity estimation work reliably for all target velocities. Therefore, we suspect that the performance drop is caused by imprecise grasp predictions of FFHNet for point clouds resulting from slow target velocities. For a conveyor belt speed of 220 mm/s, the limits of the system’s capabilities are reached.

Table I lists the success rates for each target object. High performance is achieved for many objects with varying shapes and sizes. Large cuboid objects (sugar box), sphere-like objects (apple) as well as smaller cuboid (foam brick) and cylindrical objects (cup) are grasped successfully in more than 80% of the attempts. The objects with the worst performance are the mustard bottle, the mug, and the baseball. The shape of the mustard bottle causes FFHNet to often generate grasps for its small lid requiring extremely high precision. Due to the mug’s great diameter, any deviation from the grasp pose can lead to collisions. Finally, the spherical shape of the baseball does not provide any structural features to align different perspectives. That is why the resulting model of the object represents only a fraction of the real surface which can result in insufficient grasp predictions of FFHNet.

TABLE I: Success rates of the target objects.

	Conveyor belt	Handover	Combined
Sugar box	83.3%	80%	81.8%
Pudding box	75%	100%	86.4%
Gelatin box	66.7%	100%	81.8%
Mustard bottle	41.7%	50%	45.5%
Apple	100%	60%	81.8%
Mug	50%	90%	68.2%
Baseball	58.3%	70%	63.6%
Cup	83.3%	70%	77.3%
Foam brick	91.7%	60%	77.3%
Rubik’s cube	66.7%	90%	77.3%
Overall	71.7%	77%	74.1%

TABLE II: Failure case analysis.

	Conveyor belt	Handover	Combined
Imprecise grasp pose	47.1%	82.6%	61.4%
Hand-target collision	35.3%	17.4%	28.1%
Bad grasp timing	17.6%	0%	10.5%

In Table II, the grasp failures are divided into the three cases *imprecise grasp pose*, *hand-target collision*, and *bad grasp timing*. An imprecise grasp pose resulting in an unstable grasp or miss of the target accounts for almost every second grasp failure. This case occurred most often for the mustard bottle and the baseball because FFHNet generates error-prone or inaccurate grasps for these object shapes. The reason for roughly a third of the failures is a collision of the hand with the target, most commonly observed for the mug. Its large diameter requires highly precise velocity estimation, grasp prediction, and robot control. The remaining failures are caused because a suitable hand pose was not recognized by FFHNet and the grasp was not executed at the right time. The reason can be a false prediction by FFHNet as well as inaccuracies in the construction of the virtual target model. No object is particularly affected by this case.

The plots in Figure 5 show some of the system’s quantities for a grasp of the sugar box on the conveyor belt. The linear (lin.) and rotational (rot.) errors are smoothed for better visibility and strive towards zero. The estimated (est.) velocity requires some time to converge to the ground truth value of 200 mm/s since the conveyor belt is started after the system. After 2.4 s, the visual feedback is missing and the system relies on its estimation. Tracking loss commonly occurs for large objects like the sugar box in the final approach phase because the ICP algorithm fails to reliably align the partial camera observations with the constructed virtual model. As visible in the lower plot, the success prediction (pred.) for the currently estimated state converges to the success prediction of the chosen grasp until the execution threshold is crossed. Without visual feedback, system’s grasp pose estimation still allows a successful execution of the grasp.

B. Human-to-Robot Handover

In this experiment, ten humans are asked to hand the target objects to the robot. They are instructed to hold the object on their open palm to avoid collisions between their hand and the robot’s hand. FFHNet is biased to predict top

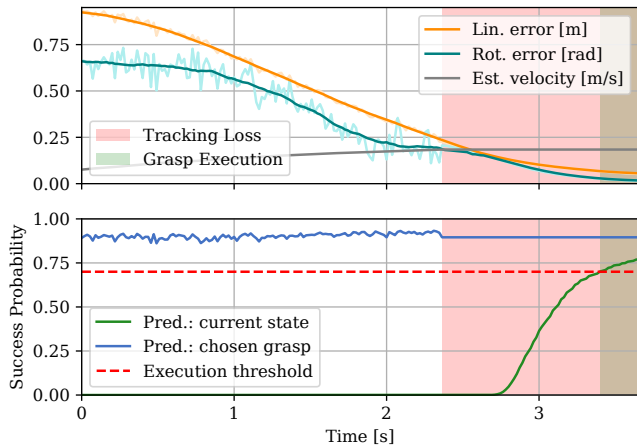


Fig. 5: Evolution of system quantities when successfully grasping the sugar box at 200 mm/s on the conveyor belt.

grasps because in its training process, grasps colliding with a virtual bottom plane were classified as unsuccessful. The target’s velocity is not estimated in this experiment assuming a constant target pose in case of tracking loss.

As listed in Table I, the overall success rate of 77% for the 100 grasp attempts is higher than the success rate of the conveyor belt experiment. This can be explained by the human habit of presenting a handover object in a way that facilitates grasping for the receiver. Consequently, many objects are grasped at success rates of 90% or higher: the pudding box, the gelatin box, and the Rubik’s cube as small and midsize cuboid objects, but also the large cylindrical mug. Interestingly, the latter is the object with the second-worst result in the conveyor belt experiment. In contrast to the conveyor belt setting, the humans’ cooperative behavior supports a precise enclosure of the object between the robotic fingers. Conversely, for the apple object and the foam brick, only 60% of the handovers are successful with them being the objects with the highest success rates in the conveyor belt experiment. The executed grasps for these items seem to be confusing for the human participants. In both experiments, the system performs worst for the mustard bottle.

As indicated by Table II, the main failure reason is an imprecise grasp pose. As for the conveyor belt experiment, this occurs most commonly for the mustard bottle because FFHNet generates error-prone grasps for the unconventional shape. The small number of hand-target collisions can be explained as humans try to avoid them during a handover. Most of these failures occurred when handing over the apple, as some of the system’s grasping attempts may have been misleading to the human participants. A delayed execution never led to grasp failure in this experiment.

Figure 6 shows the minimization of the linear and rotational errors and the increase of the success prediction for a successful handover of the Rubik’s cube without significant tracking loss.

V. CONCLUSION & FUTURE WORK

We presented a system to grasp unknown dynamic objects with a multi-fingered hand which we believe is an

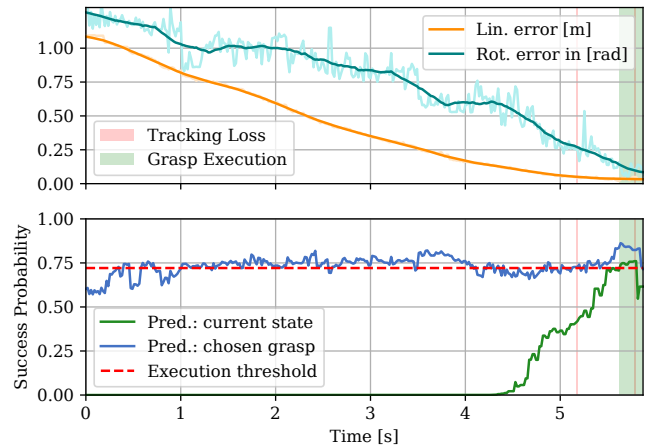


Fig. 6: Evolution of the system quantities for a successful handover of the Rubik’s cube.

unprecedented achievement. It constructs a virtual target model by processing camera data from a single view with a visual object tracking model, ICP, and further filtering. This model constitutes the input to the generative grasping model FFHNet, providing a distribution of possible grasps. Considering their related success predictions as well as other environmental quantities, the most suitable grasp is selected and continuously updated in real-time. The virtual model and velocity estimation enable the system to compensate for missing visual feedback in case of tracking loss or alignment errors of the observed camera data. In our conducted experiments with real hardware, the system grasped various dynamic objects in different challenging scenarios at a remarkable overall success rate of 74.1%.

The reasons for the most common failure case, a grasp execution with an imprecise hand pose, are insufficient target model creation and inaccurate predictions of FFHNet. To further improve the system’s precision, a more robust approach to construct the target model than visual object tracking + ICP as well as a more reliable generative grasping model than FFHNet is required. This will also reduce the number of failures due to bad grasp timing, as the underlying reasons are similar.

Additionally, with an approach capable of generating a diverse distribution of suitable grasps, the grasp metric can be extended to also evaluate the direction of the target movement. Approaching the target from the direction in which it is moving facilitates dynamic grasping [21]. With FFHNet, this is not possible due to its top-grasp bias.

The remaining failure cases due to hand-target collisions can be addressed by implementing real-time capable trajectory planning and collision checking. However, this requires a reliable creation of the virtual target model.

ACKNOWLEDGMENT

This research has received funding from the European Union’s Horizon 2020 research and innovation programme under the Marie Skłodowska-Curie grant agreement No 778602 ULTRACEPT.

REFERENCES

- [1] H. Liu, K. Wu, P. Meusel, N. Seitz, G. Hirzinger, M. Jin, Y. Liu, S. Fan, T. Lan, and Z. Chen, "Multisensory five-finger dexterous hand: The dlr/hit hand ii," in *2008 IEEE/RSJ International Conference on Intelligent Robots and Systems (IROS)*, 2008, pp. 3692–3697.
- [2] N. Y. Lii, Z. Chen, B. Pleintinger, C. H. Borst, G. Hirzinger, and A. Schiele, "Toward understanding the effects of visual- and force-feedback on robotic hand grasping performance for space teleoperation," in *2010 IEEE/RSJ International Conference on Intelligent Robots and Systems (IROS)*, 2010, pp. 3745–3752.
- [3] Z. Chen, N. Lii, T. Wimböck, S. Fan, H. Liu, and A. Albu-Schäffer, "Experimental analysis on spatial and cartesian impedance control for the dexterous dlr/hit ii hand," *International Journal of Robotics and Automation*, vol. 29, p. 1 12, 01 2014.
- [4] V. Mayer, Q. Feng, J. Deng, Y. Shi, Z. Chen, and A. Knoll, "Ffhnet: Generating multi-fingered robotic grasps for unknown objects in real-time," in *2022 International Conference on Robotics and Automation (ICRA)*, 2022, pp. 762–769.
- [5] F. Husain, A. Colomé, B. Dellen, G. Alenyà, and C. Torras, "Realtime tracking and grasping of a moving object from range video," in *2014 IEEE International Conference on Robotics and Automation (ICRA)*, 2014, pp. 2617–2622.
- [6] X. Ye and S. Liu, "Velocity decomposition based planning algorithm for grasping moving object," in *2018 IEEE 7th Data Driven Control and Learning Systems Conference (DDCLS)*, 2018, pp. 644–649.
- [7] T.-H. Pham, G. De Magistris, and R. Tachibana, "Oplayer - practical constrained optimization for deep reinforcement learning in the real world," in *2018 IEEE International Conference on Robotics and Automation (ICRA)*, 2018, pp. 6236–6243.
- [8] Z. Tu, C. Yang, X. Wu, Y. Zhu, W. Wu, and N. Jia, "Moving object flexible grasping based on deep reinforcement learning," in *2022 8th International Conference on Control, Automation and Robotics (ICCAR)*, 2022, pp. 34–39.
- [9] N. Houshangi, "Control of a robotic manipulator to grasp a moving target using vision," in *Proceedings., IEEE International Conference on Robotics and Automation (ICRA)*, 1990, pp. 604–609 vol.1.
- [10] P. Allen, A. Timcenko, B. Yoshimi, and P. Michelman, "Automated tracking and grasping of a moving object with a robotic hand-eye system," *IEEE Transactions on Robotics and Automation (T-RO)*, vol. 9, no. 2, pp. 152–165, 1993.
- [11] C. Smith and N. Papanikolopoulos, "Grasping of static and moving objects using a vision-based control approach," in *Proceedings 1995 IEEE/RSJ International Conference on Intelligent Robots and Systems (IROS). Human Robot Interaction and Cooperative Robots*, vol. 1, 1995, pp. 329–334 vol.1.
- [12] H. Nomura and T. Naito, "Integrated visual servoing system to grasp industrial parts moving on conveyer by controlling 6dof arm," in *2000 IEEE International Conference on Systems, Man and Cybernetics (SMC)*, vol. 3, 2000, pp. 1768–1775 vol.3.
- [13] J. Fuentes-Pacheco, J. Ascencio, and J. Rendon-Mancha, "Binocular visual tracking and grasping of a moving object with a 3d trajectory-predictor," *Journal of Applied Research and Technology*, vol. 7, p. 259, 12 2009.
- [14] S. Escalda Navarro, D. Weiss, D. Stogl, D. Milev, and B. Hein, "Tracking and grasping of known and unknown objects from a conveyor belt," in *ISR/Robotik 2014; 41st International Symposium on Robotics*, 2014, pp. 1–8.
- [15] P. Arora and C. Papachristos, *Mobile Manipulator Robot Visual Servoing and Guidance for Dynamic Target Grasping*. Springer International Publishing, 12 2020, pp. 223–235.
- [16] D. Morrison, P. Corke, and J. Leitner, "Closing the loop for robotic grasping: A real-time, generative grasp synthesis approach," *CoRR*, vol. abs/1804.05172, 2018.
- [17] D. Morrison, P. Corke, and J. Leitner, "Learning robust, real-time, reactive robotic grasping," *The International Journal of Robotics Research*, vol. 39, pp. 183 – 201, 2019.
- [18] M. Tuscher, J. Hörz, D. Driess, and M. Toussaint, "Deep 6-dof tracking of unknown objects for reactive grasping," 2021.
- [19] N. Marturi, M. Kopicki, A. Rastegarpanah, V. Rajasekaran, M. Adjigble, R. Stolkin, A. Leonardis, and Y. Bekiroglu, "Dynamic grasp and trajectory planning for moving objects," in *Autonomous Robots*, 2019, pp. 1241–1256.
- [20] C. De Farias, M. Adjigble, B. Tamadazte, R. Stolkin, and N. Marturi, "Dual quaternion-based visual servoing for grasping moving objects," in *2021 IEEE 17th International Conference on Automation Science and Engineering (CASE)*, 2021, pp. 151–158.
- [21] I. Akinola, J. Xu, S. Song, and P. K. Allen, "Dynamic grasping with reachability and motion awareness," 2021.
- [22] C.-C. Wong, M.-Y. Chien, R.-J. Chen, H. Aoyama, and K.-Y. Wong, "Moving object prediction and grasping system of robot manipulator," *IEEE Access*, vol. 10, pp. 20 159–20 172, 2022.
- [23] H.-S. Fang, C. Wang, H. Fang, M. Gou, J. Liu, H. Yan, W. Liu, Y. Xie, and C. Lu, "Anygrasp: Robust and efficient grasp perception in spatial and temporal domains," *IEEE Transactions on Robotics (T-RO)*, pp. 1–17, 2023.
- [24] P. Rosenberger, A. Cosgun, R. Newbury, J. Kwan, V. Ortenzi, P. Corke, and M. Grafinger, "Object-independent human-to-robot handovers using real time robotic vision," *IEEE Robotics and Automation Letters (RA-L)*, vol. 6, pp. 17–23, 01 2021.
- [25] W. Yang, C. Paxton, A. Mousavian, Y.-W. Chao, M. Cakmak, and D. Fox, "Reactive human-to-robot handovers of arbitrary objects," in *2021 IEEE International Conference on Robotics and Automation (ICRA)*, 2021, pp. 3118–3124.
- [26] P. Chen and W. Lu, "Deep reinforcement learning based moving object grasping," *Information Sciences*, vol. 565, pp. 62–76, 2021.
- [27] M. Kristan, J. Matas, A. Leonardis, M. Felsberg, R. Pflugfelder, J.-K. Kamarainen, H. J. Chang, M. Danelljan, L. Čehovin Zajc, A. Lukežič, O. Drbohlav, J. Kapyla, G. Hager, S. Yan, J. Yang, Z. Zhang, G. Fernandez, and et. al., "The ninth visual object tracking vot2021 challenge results," 2021.
- [28] P. Besl and N. D. McKay, "A method for registration of 3-d shapes," *IEEE Transactions on Pattern Analysis and Machine Intelligence*, vol. 14, no. 2, pp. 239–256, 1992.
- [29] Y. Chen and G. Medioni, "Object modelling by registration of multiple range images," *Image and Vision Computing*, vol. 10, no. 3, pp. 145–155, 1992.
- [30] S. Prokudin, C. Lassner, and J. Romero, "Efficient learning on point clouds with basis point sets," 2019.
- [31] R. E. Kalman, "A new approach to linear filtering and prediction problems," *Transactions of the ASME—Journal of Basic Engineering*, vol. 82, no. Series D, pp. 35–45, 1960.
- [32] B. Calli, A. Walsman, A. Singh, S. Srinivasa, P. Abbeel, and A. M. Dollar, "Benchmarking in manipulation research: Using the yale-CMU-berkeley object and model set," *IEEE Robotics Automation Magazine (RAM)*, vol. 22, no. 3, pp. 36–52, sep 2015.